
Effect of In-Plane Voiding on the Fracture Behavior of Laser Sintered Polyamide

David K. Leigh, David L. Bourell, Joseph J. Beaman Jr.

The University of Texas at Austin, USA

Harvest Technologies, Inc., USA

REVIEWED, August 17 2011

ARTICLE INFO

Keywords:

Additive Manufacturing (AM)

Rapid

Polyamide

Selective Laser Sintering (SLS)

ABSTRACT

The primary contributors to poor mechanical properties in polyamide materials used during Selective Laser Sintering® are qualified. Methods to quantify the decreased mechanical properties, including Scanning Electron Microscopy (SEM) of fracture surfaces, are compared against each other and against mechanical properties of components fabricated using multiple process parameters. Of primary interest are Ultimate Tensile Strength (UTS) and Elongation at Break (EOB) of tensile specimens fabricated under conditions that produce varying degrees of ductile and brittle fracture.

INTRODUCTION

Laser Sintering

Additive manufacturing is a family of relatively new manufacturing processes utilizing integration techniques of digital solid models and the layer-by-layer addition of materials to create a three-dimensional solid. Selective Laser Sintering®, developed at The University of Texas at Austin, utilizes three major steps to create the three-dimensional solid. The first step of the process is the computational evaluation the solid model and the subsequent creation of a set of cross-sectional vectors referred to as “slices,” with each slice having a field of x-y vectors that represent the cross-sectional area of the model. Each slice is prepared based upon a predetermined “layer thickness” which is typically 0.004” to 0.010”. The second step of the process is to preheat a bed of powder, commonly a polyamide (nylon) material with an average particle size of 50 microns. Once the powder is heated to a sufficient temperature and the slice file is created, a directed energy beam (CO₂ laser) scans the vector field on the prepared bed of powder. The fused layer reproduces the cross-section generated by the vector field (or slice). Once fused, a layer of powder equal to the predetermined layer thickness is added, heated, and subsequently fused to prior layers to create a solid physical model, illustrated in Figure 1.

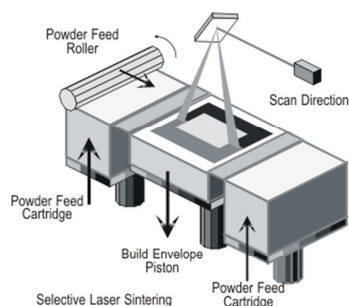


Fig 1: Selective Laser Sintering® Process

Adaptation of Laser Sintering for End-Use Parts

The laser sintering process has become accepted as the most robust additive manufacturing process and has been deemed suitable for the production of end-use parts in a number of applications. This novel technique has allowed for streamlined design, decreased time to productize, minimal cost on engineering changes, and the ability to design for function rather than manufacturability. While there may be many benefits for certain applications, there are significant challenges that must be addressed prior to a broad acceptance of this technology. The key challenge is the limited amount of theoretical or experimental science specific to use of laser sintering as a manufacturing process.

Process Variability and Limitation of Mechanical Properties

A significant limitation to any layer-based additive manufacturing process is the anisotropic nature of the process. In this case, a single layer (typically 0.004” thick) is fused for each layer. The properties within this layer are fairly consistent, but the bond between layers is typically viewed as weak. This is quantified through the placement of standard ASTM tensile specimens oriented in the X-axis (left to right), Y-axis (front to back), and Z-axis (vertical build direction). It is typically observed that there is little to no variation between the X and Y axes, but that the Z-axis will yield a significantly lower elongation at break (EOB) than is observed in the X and Y axes.

The primary cause of the lower mechanical properties in the Z-axis can be attributed to layer-to-layer adhesion. There are several causes of this effect, but little has been done to illustrate what is actually happening. To illustrate the effect of material processing on mechanical properties, several techniques are used. As to the cause of poor adhesion between layers, there are several factors that may contribute to this:

Large layer size – The powder insulates the thermal energy and prevents the energy of the beam from penetrating to the prior layer.

Poor powder quality – Used powder will yield a higher melt-flow and higher molecular weight. This is primarily caused through thermal aging and cross-linking of the polymer. The result of the higher melt-flow is a polymer that is slow to melt and prone to the creation of voids.

Poor thermal control – If the powder bed is processed in a way that the temperature is too low or is cooled at a high rate, it will inhibit the formation of a melt pool that penetrates the previous layer. The result can be weak layer-to-layer adhesion as well as dimensional distortions.

Low laser energy – High scan speed, low laser power, and large spacings between scan vectors can lower the overall laser energy delivered to the powder bed. This decreased energy will not yield sufficient layer-to-layer adhesion.

Formation of Layers in Laser Sintering

Figure 2 is a graphical representation of the raw material powder bed. While the average particle size of the polyamide material is 50 microns, there is a range of fine particles in a randomly packed bed. This powder bed is preheated to a point just below the melting temperature. If the particles are too hot, they will pool and there will be no distinction between the scanned area and the powder bed. If the particles are too cold, they will not have sufficient internal energy to allow for a full melt. In addition, a region heated primarily through laser energy will have significant dimensional distortion as the fused layer rapidly cools and shrinks. Subsequent layers that are fused will try to shrink, creating residual stresses due to adhesion with previous layers.

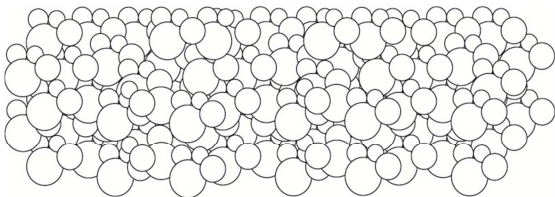


Figure 2: Cross Section of a Laser Sintering Powder Bed

Once the powder bed has been pre-heated, the laser will scan the subject cross-section using a field of x-y vectors at a prescribed speed, spacing, and laser power. These settings are optimized to yield an ideal melt pool such that there is sufficient energy to have a full melt without losing precision. If the laser energy applied is too great, detail and precision are lost (analogous to writing on tissue paper with a large permanent marker.) Figure 3 illustrates the melting of the powder bed surface by the laser. There is a corresponding depth of penetration directly proportional to the laser energy applied.

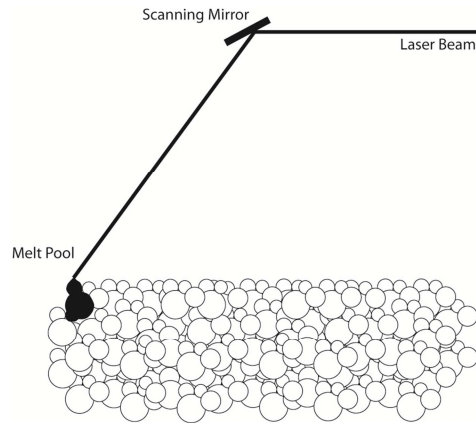


Figure 3: Melt Pool Generated on a Powder Bed

EXPERIMENTAL PROCEDURE

Design of Experiments to Evaluate and Correlate Physical and Visual Properties

The objective of this research is to correlate the mechanical properties observed with visual inspection to obtain a better understanding of the failure mechanisms of laser sintered parts. The material was 3D Systems Duraform® PA, a Nylon 12 polyamide. Tensile specimens were added to a production build to evaluate the surface of a tensile specimen and the fracture surfaces of both X and Z direction tensile specimens. The process settings and build location of test specimens were such that the three failure modes typical for laser sintering would be present for this experiment:

1. Delamination – A failure that is characterized by very weak layer-to-layer adhesion. The fracture of a z-axis oriented tensile specimen will break exclusively in the region between layers. Delaminated Z-direction tensile specimens were processed at standard thermal parameters with laser power at less than 50% of recommended parameters.
2. Brittle Fracture – Failure typically characterized with ultimate tensile strength and offset yield strength comparable to stated material datasheets, yet with a significant reduction in elongation at break. Processing parameters are what is typical for most prototype builds.
3. Ductile Fracture – This is the desired failure mode. A ductile fracture will yield nearly isotropic parameters. Processing parameters have been optimized for build quality with a sacrifice in efficiency and cost.

Observation and Quantification of Actual Tensile Specimen Failure

Tensile properties were measured using an MTS Insight 10 at Harvest Technologies. The specimens produced were ASTM D638 specimens with a cross-sectional area at fracture of roughly 0.125" X 0.500". The procedure for pulling the specimens was to use a 0.20 inch/minute rate with an extensometer that conforms to ASTM E83 class B2 with a range of at least 50%.

The fracture surface was evaluated using a JEOL JSM 5610 Scanning Electron Microscope (SEM) at The University of Texas at Austin with a Tungsten filament, 3nm resolution, and magnification up to 300,000 times.

A total of 24 specimens were produced and evaluated. These specimens were segregated based on the tensile results, with selected samples being evaluated using SEM. Specimens were sputtered after tensile testing and prior to evaluation in the SEM. 8 of the 24 specimens were used with redundant specimen data being discarded.

Evaluation of Melt Flow Rate on Tensile Specimen Failure Using Injection Molding

It has been observed that a primary contributor to poor mechanical properties of laser sintered components is the thermal aging, or degradation, of the material. Continuous exposure of the un-sintered material to the elevated thermal environment causes cross-linking in the polymer chain and contributes to decreased physical and mechanical properties. As the material undergoes thermal aging, the viscosity of the material is seen to increase and can be evaluated using a melt-flow measurement tool.

A key consideration in evaluating tensile specimen failure is whether this material degradation is an intrinsic material defect or whether this change in viscosity has an effect on process specific layer-to-layer adhesion. Unusable polyamide powder was segregated from production at Harvest Technologies and its viscosity (melt flow rate) evaluated. This used polyamide powder was then processed in an injection molding machine at The University of Texas to produce several tensile coupons.

Geometric Consideration of the Interface Boundary Layer

When laser sintered specimens are observed optically, there is a visible boundary layer between subsequently fused layers. This boundary layer is exclusively seen in the X-Y plane. This interface boundary layer appears to be the primary culprit in decreased mechanical properties and can be characterized as a layer of coplanar voids. Therefore, tensile specimens were created using CAD to simulate this boundary layer with varying degrees of severity. These specimens were then processed in the stronger X-direction in order to isolate the effect of the decreased z-direction mechanical properties on this experiment.

Figure 3 illustrates the CAD model that was created to simulate coplanar powder particles. The tensile bar was scaled up from a standard ASTM D638 tensile bar the particle diameter was modeled at 0.100".

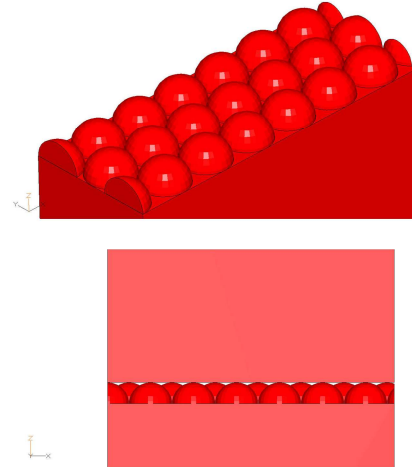


Figure 4: Coplanar spheres and voids

The two halves of the tensile bar were created independently in order to allow for a variation in the interface interference between a plane on one half and coplanar spheres on the other. This interface will be defined by an "h/r Ratio" seen in Figure 5. An h/r Ratio of 0 will have the spheres just touching the plane as illustrated in Figure 4. A ratio of 1 will have no effective interface boundary and is equivalent to a solid tensile bar. Eleven tensile specimens were produced with an h/r Ratio from 0 to 1 at an increment of 0.1. The material used was a polyamide 11 in an optimized production build. Optimized polyamide 11 production builds typically yield the highest mechanical properties and should provide the greatest contract for the varying h/r ratio tensile specimens.

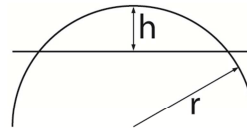


Figure 5: h/r Ratio

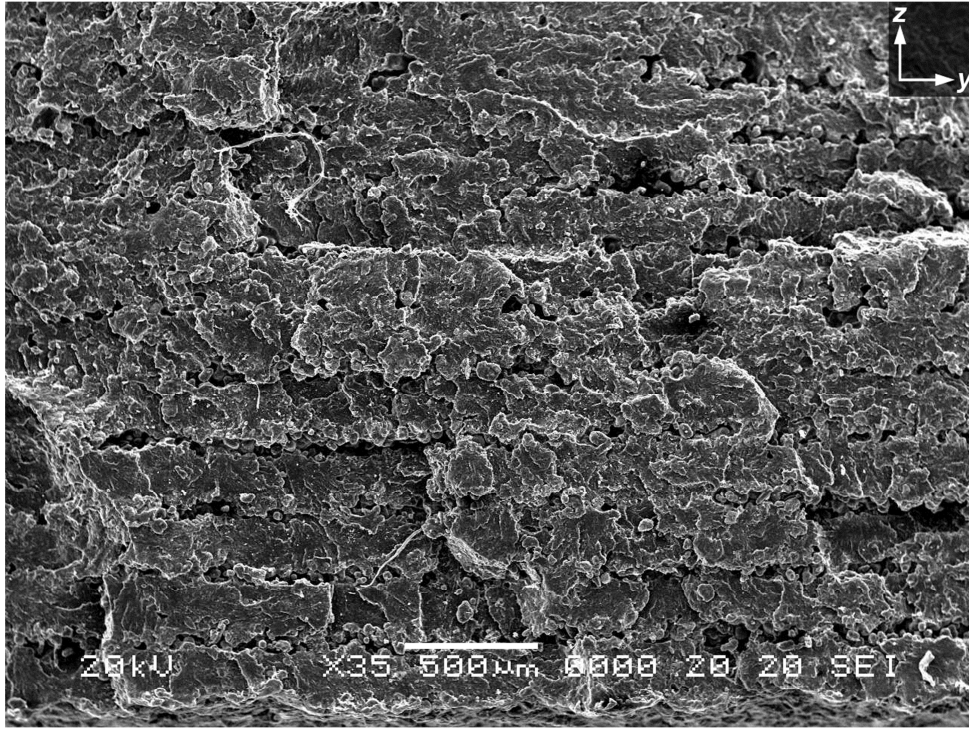


Figure 6: SEM of X Tensile Bar Fracture Surface. (35x)

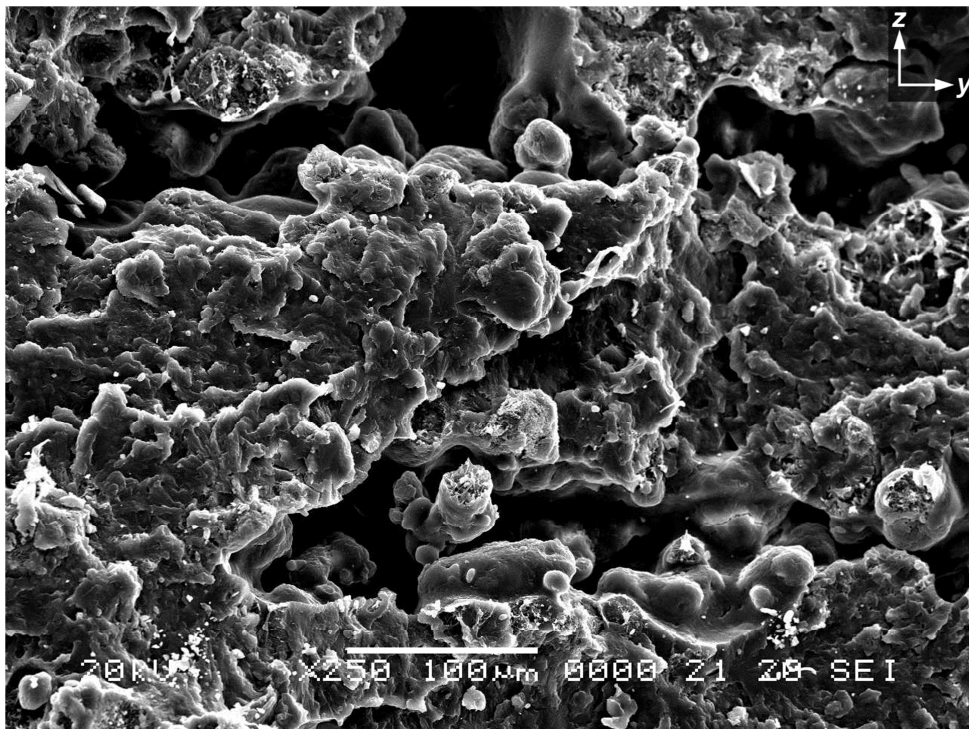


Figure 7: SEM of X Tensile Bar Fracture Surface. (250x)

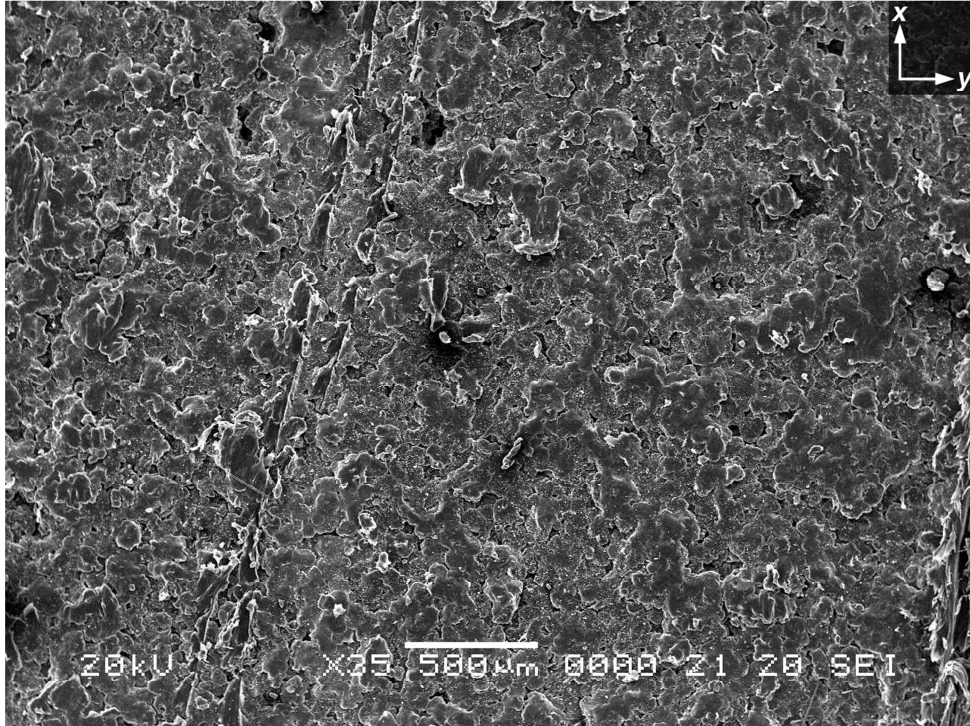


Figure 8: SEM of X Tensile Bar Top-Facing Surface. (35x)

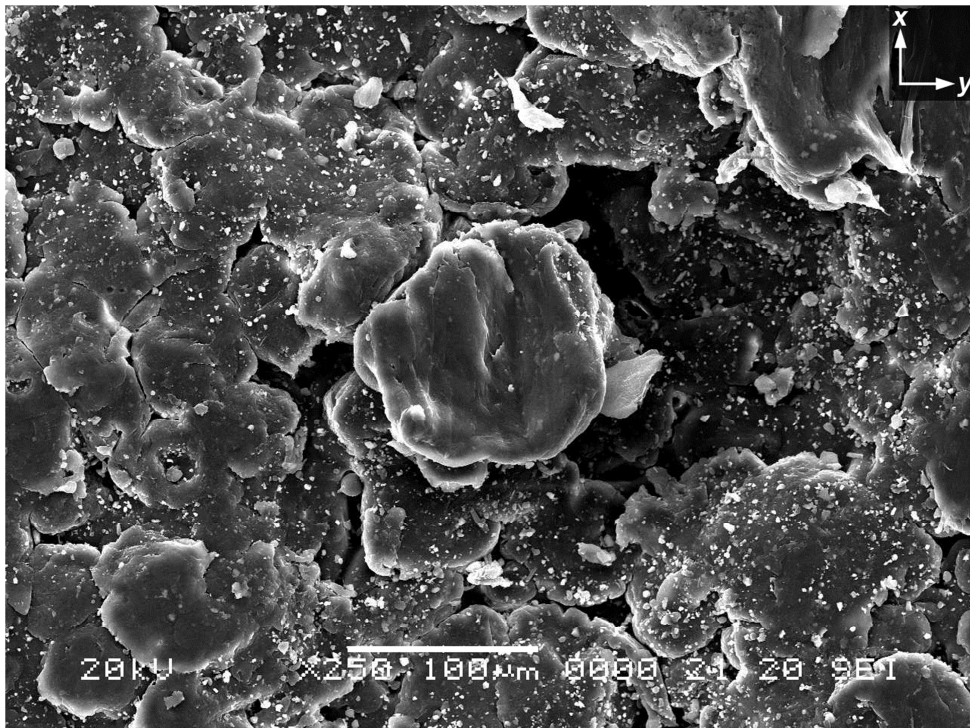


Figure 9: SEM of X Tensile Bar Top-Facing Surface. (250x)

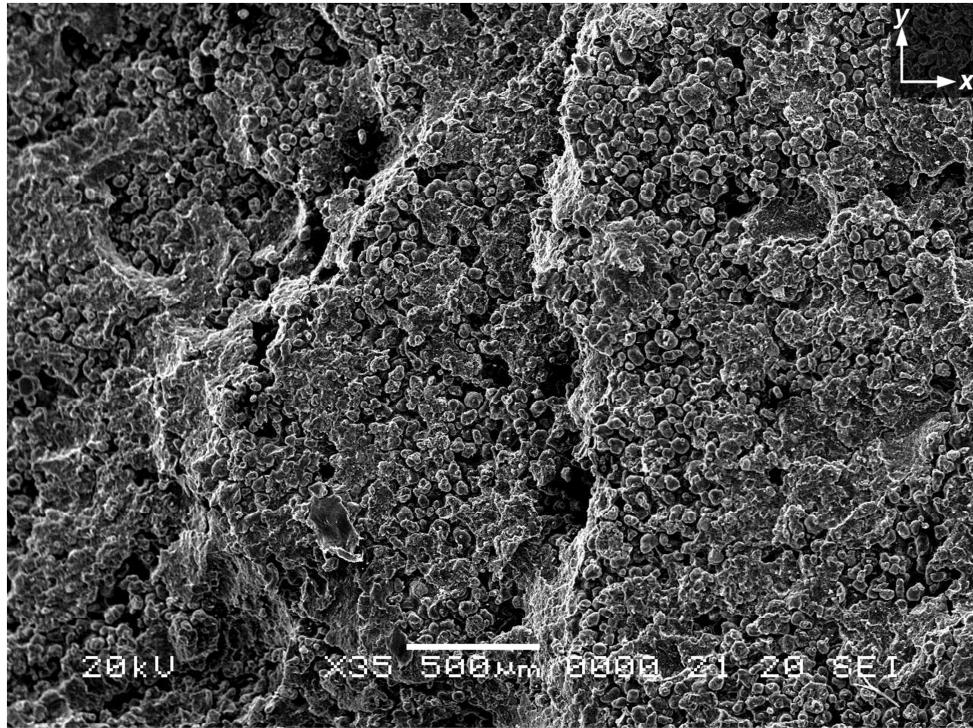


Figure 10: SEM of Z Tensile Bar - Delamination. (35x)

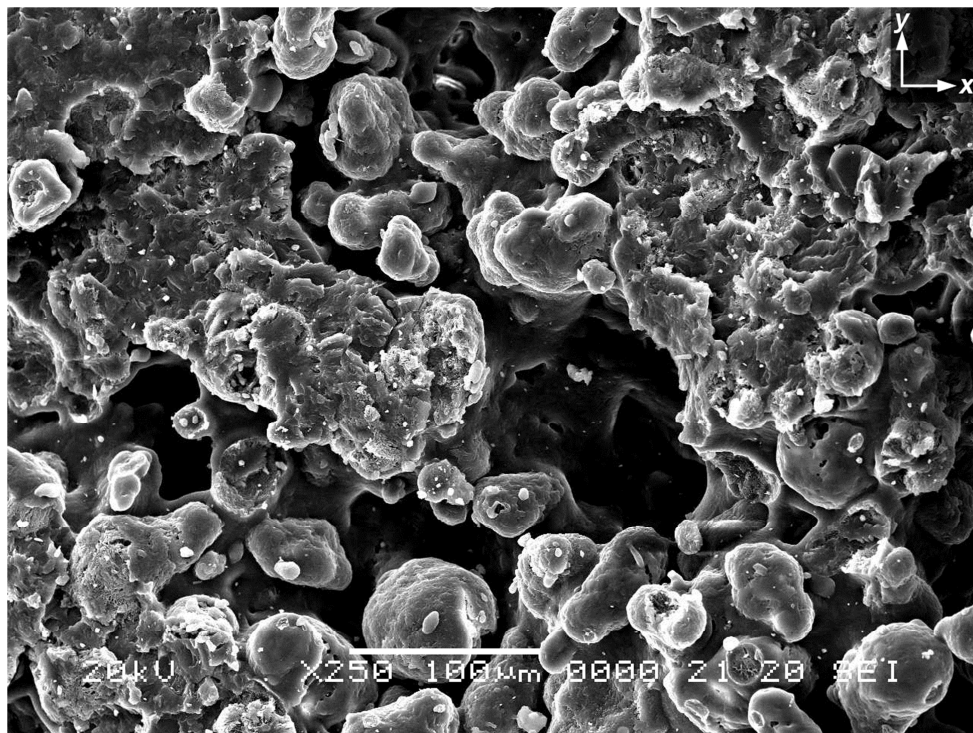


Figure 11: SEM of Z Tensile Bar - Delamination. (250x)

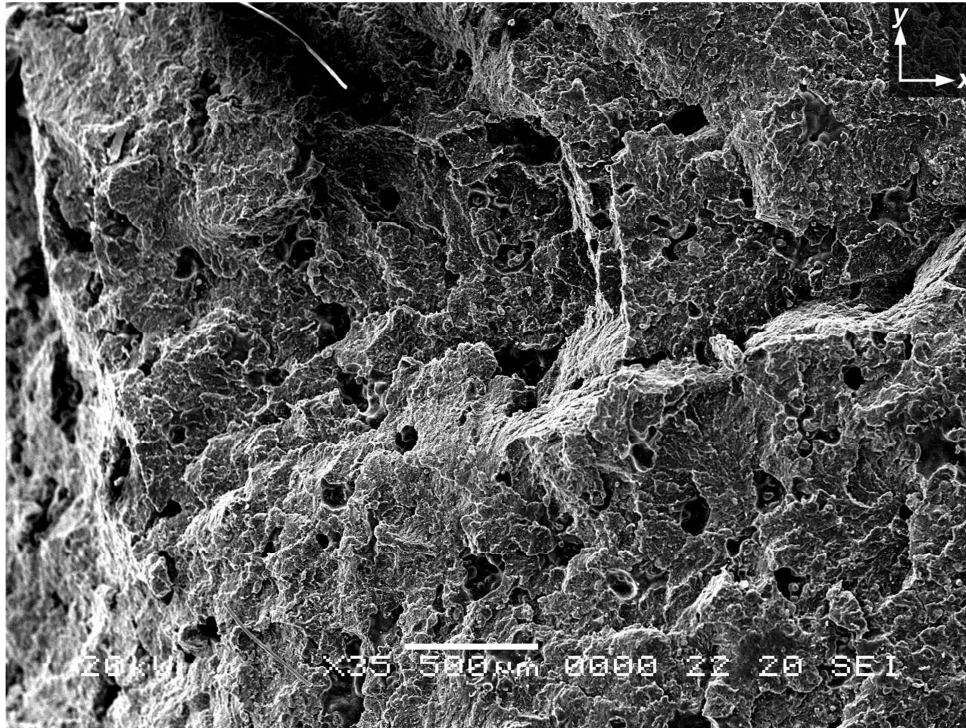


Figure 12: SEM of Z Tensile Bar – Brittle Fracture. (35x)

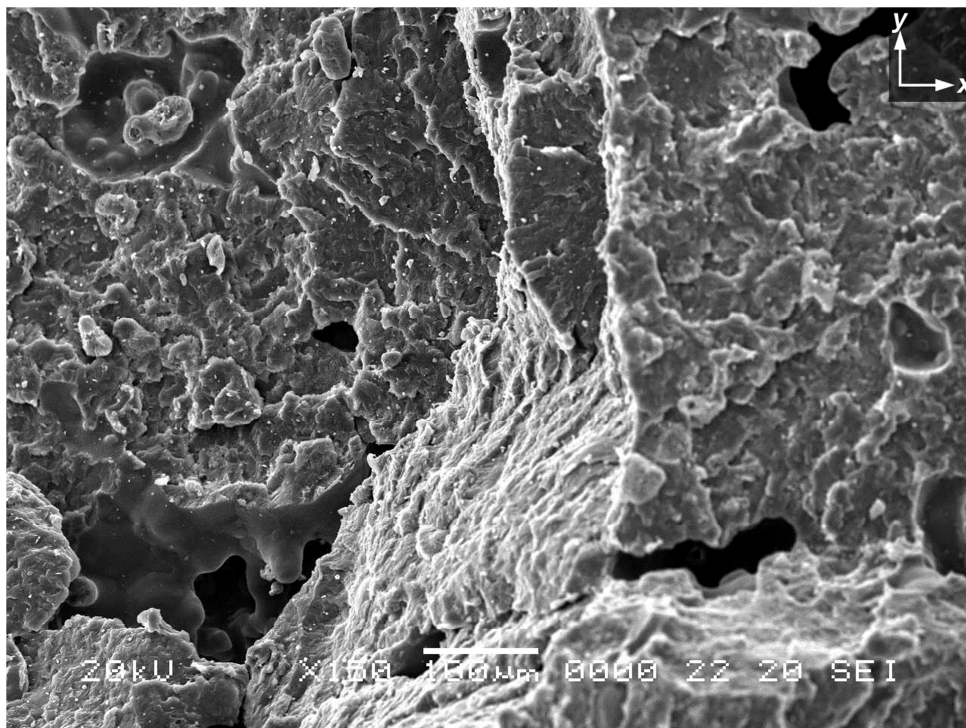


Figure 13: SEM of Z Tensile Bar - Brittle Fracture. (250x)

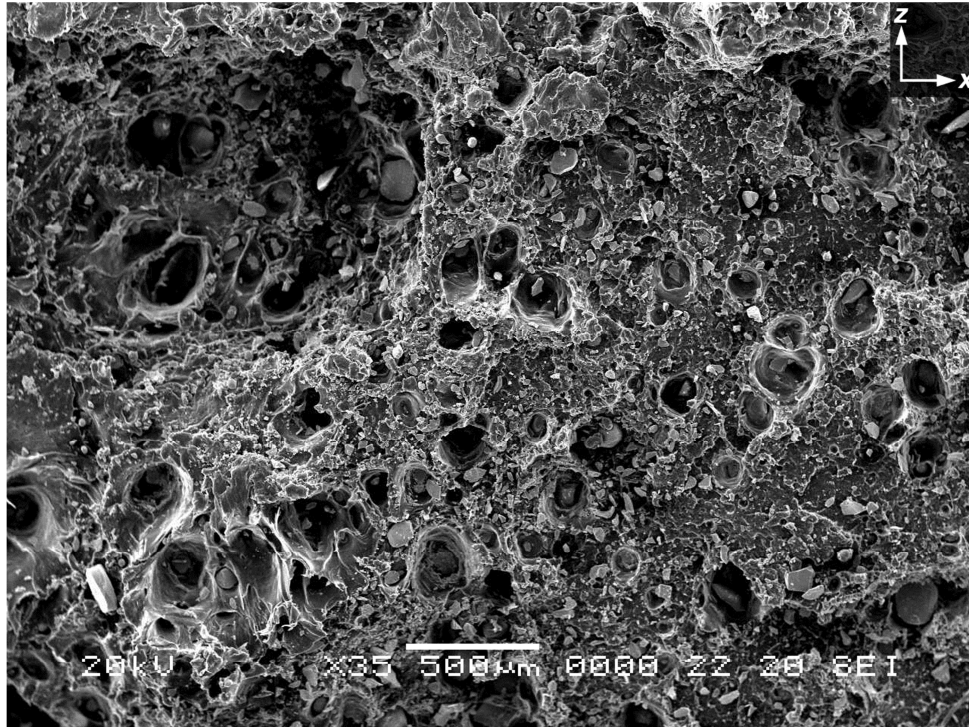


Figure 14: SEM of Y Tensile Bar - Ductile Fracture. (35x)

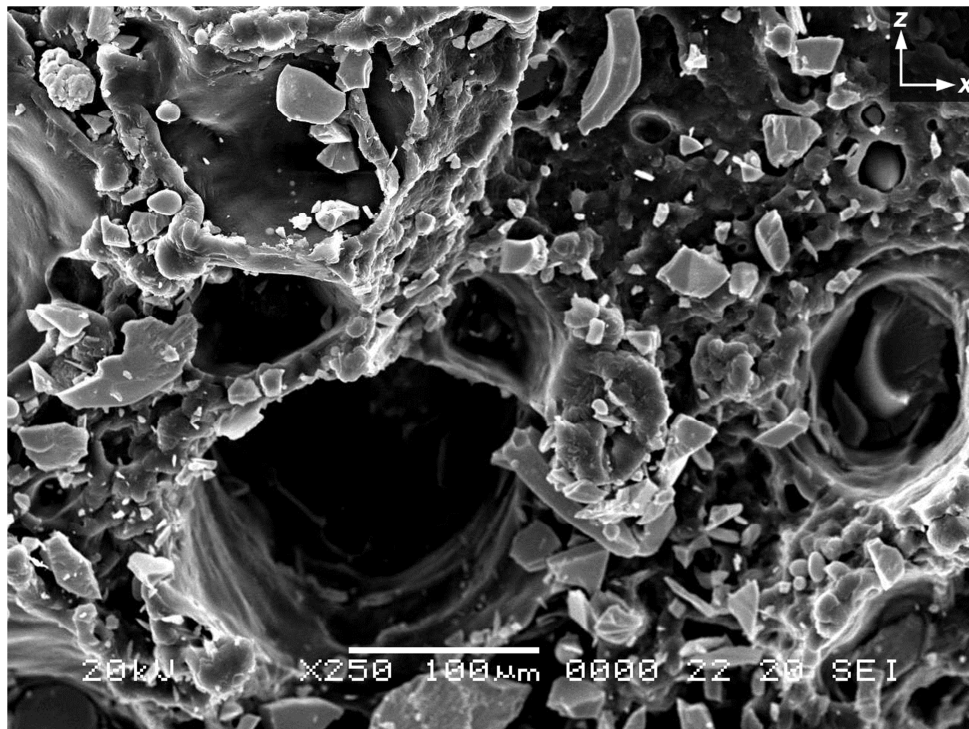


Figure 15: SEM of Y Tensile Bar - Ductile Fracture. (250x)

RESULTS

The tensile testing performed yielded the results illustrated in Table 1. A data from 8 specimens is listed in this table and illustrated in the SEM photographs. Tensile specimen nomenclature identifies the geometric location of the sample in the build as well as the build orientation. A “zx” specimen would be oriented primarily in the z-axis with the secondary axis oriented in the x-axis. An “x” specimen would be oriented flat in the x-y plane with the primary length along the x-axis. The x-axis specimens yield both better mechanical properties and consistent results.

Table 1: Tensile Properties and Fracture Mode

Sample	Ultimate Tensile Strength (UTS)	Elongation at Break (EOB)	Fracture Mode
ZX 12.0.3	494 psi	1%	Delamination
ZX 0.0.3	2969 psi	1%	Delamination
ZX 0.12.3	1278 psi	1%	Delamination
ZX 13.11.3	5164 psi	3%	Brittle
X 4.2.8	5886 psi	7%	Brittle
X 4.3.8	5991 psi	6%	Brittle
X 4.4.8	5763 psi	7%	Brittle
+Y 1.4.0 ¹	6099 psi	44%	Ductile

¹ Ductile fracture taken from independently optimized build.

Morphology

The SEM image shown in Figure 6 shows clear patterns for the layers with elongated horizontal voids between layers. Figure 7 is a magnified region of the same sample. It illustrates a single layer with voids both above and below the fully melted layer. There are also fully dense regions where there was sufficient energy to melt the layers together, creating a more homogeneous region.

The surface of an XY tensile specimen is illustrated in Figures 8 and 9. This shows the upper facing surface and the surface to which the loose powder must be bonded by the laser. The average particle size is roughly 50 microns and individual particles can be seen to be melted in Figure 9, appearing like a lily pad or pancake structure. Some particles can be seen to have melted with other particles while others appear to be isolated with voids between particles. Of particular interest in Figure 9 is the 250 μ m boulder looking particle in the center of the micrograph.

The fracture surfaces of the Z tensile specimens are shown in Figures 10 through 15. Delamination is illustrated in Figures 10 and 11, brittle fracture in Figures 12 and 13, and ductile fracture in Figures 14 and 15.

Injection Molded Tensile Specimens

Standard injection molding parameters from a materials handbook were used to create fully dense ASTM D638 tensile specimens. This particular machine was not in the greatest state of repair, but was sufficient in creating several tensile specimens from the used material. The powder was poured directly into the extruder and processed manually. The results of the tensile test is presented in Table 2. Both specimens exceeded the range of the extensometer (50%) with one specimen pulled until it reached the mechanical limits of the load cell.

Table 2: Injection Molded Tensile Results

Sample	Ultimate Tensile Strength (UTS)	Elongation at Break (EOB)	Fracture Mode
Sample 1	5572 psi	>50%	Ductile
Sample 2	5530 psi	>200%	Ductile

h/r Ratio Tensile Specimens

Two builds of 11 samples each were built and evaluated, with one set of samples having a finished surface and the other set having no post finishing done. There was no difference in ultimate tensile strength and elongation between builds. The data presented in Table 3 and Figure 16 is from the natural tensile specimens.

Table 3: h/r Ratio Tensile Results

Sample	h/r Ratio	σ_y (psi)	UTS (psi)	EOB %
1	0	2772	2954	4
2	0.1	2854	3124	4
3	0.2	3028	4021	6
4	0.3	3056	4976	7
5	0.4	3163	5312	9
6	0.5	3047	5468	9
7	0.6	2824	5882	17
8	0.7	3090	6130	17
9	0.8	3225	5994	16
10	0.9	3214	6133	18
11	1.0	3015	7391	>50*

* Specimen exceeded extensometer limit of 50%.

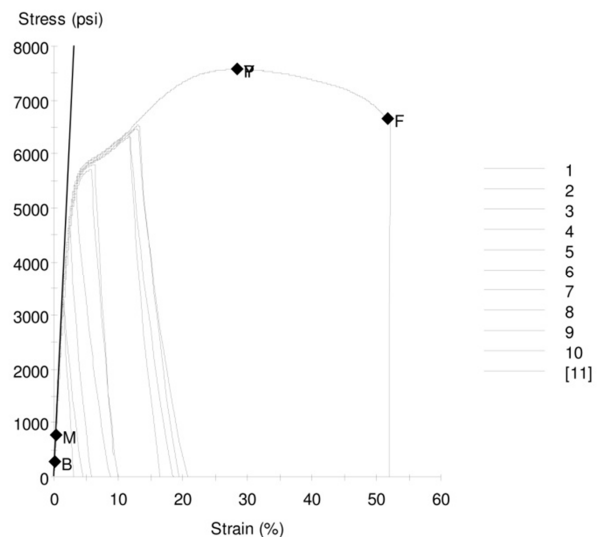


Figure 16: Stress-Strain Curve for h/r Ratio Specimens

DISCUSSION

[Figure 6] With the understanding that the z-axis is the primary direction for added layers, a pattern of voids between layers is apparent. This stratification contributes to anisotropic material properties and significant weakness if a tensile stress is exerted parallel to the z-axis. In addition, these patterns of voids contribute to a significant reduction in elongation and ultimate tensile strength.

[Figure 9] It appears that the $250\mu\text{m}$ particle was formed when several particles melted together but did not fully adhere to the surface. When the particles cooled, there became a condensed grouping of several melted particles with a surrounding void. This voided region may contribute to voids in the part unless sufficient energy is used to re-melt these particles and bond with the

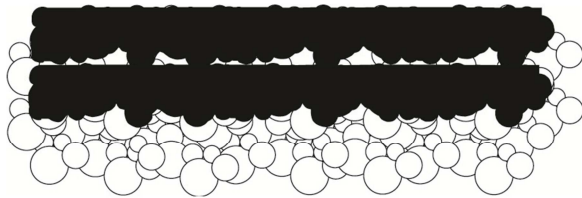


Figure 16: Lightly adhered layers contributing to delamination.

surrounding surface.

It is apparent from the analysis of these samples that the cracks propagate through voids created by a lack of full melt between layers. The general observations for each fracture mode are listed below:

[Figures 10 and 11] These images show a fracture of the Z specimen

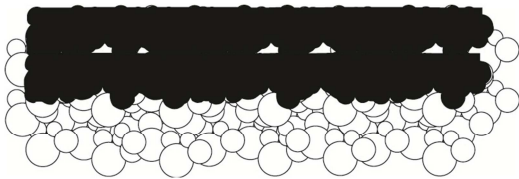


Figure 17: Incomplete fusion contributing to brittle fracture.

that is parallel to the x-y plane. Three distinct layers are represented as the crack propagation followed the area between two parallel layers and then migrated to neighboring layers. This pattern, when

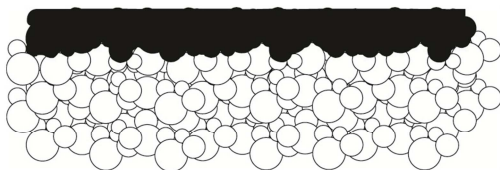


Figure 18: Initial Layer of Sintered Powder

examined in Figure 11 shows that the particles are roughly 50 microns in diameter, which corresponds to the average particle size of the raw material. When compared to the morphology of the top layer (Figures 8 and 9), it can be seen that the bottom layer has very little bonding to the previous layer.

[Figures 12 and 13] Voids are isolated and somewhat periodic, with similar size and spacing. Fracture surfaces show a ductile tear with trans-granular fractures or river marks. These fracture surfaces are similar to the ductile specimen (Figure 14) but with void fraction on the failure surface higher.

[Figures 14 and 15] With an elongation of 44%, it may be observed that there is void nucleation where the material tore apart from itself. From Figure 15 shards of material and a very dense surface are observed.

It is apparent that the material properties observed in Table 1 can be correlated to the extent of voids present between sintered layers. With very little adhesion between layers, delamination and elongation values near 1% are seen. With sufficient energy to melt through the target layer into the previous layer, a fully dense part will yield elongations well above 10%. As the layer has a higher degree of melt, the voids will decrease through the brittle range until the voids no longer contribute to the fracture.

Figures 3 and 4 are illustrations of two subsequently built layers with voids being created between layers through the lack of complete particle melt to the previous layer. Figure 17 shows a larger separation between layers and represents the sample seen in Figures 10 and 11 (delamination). Since the voids are coplanar, they are analogous to pre-existing cracks. The crack propagation in this example will cause a shear between layers resulting in delamination.

Figure 18 represents the sample seen in Figures 12 and 13 (brittle fracture) with voids present, but with the voids being isolated and periodic. The crack propagation in this example is much less directional since the voids are no longer exclusively coplanar. A fracture may originate between specific layers, but will typically travel through voids in neighboring layers since the distribution of voids is much less ordered.

Figure 18 is a graphical representation of an initial layer created in the laser sintering process. The depth of this layer is dependant upon the laser energy, but regardless of the amount of energy on the first layer, the downward facing surface will be defined by the raw material particle size as seen in Figure 10. The top of the layer is flat and will look like the surfaces seen in Figure 8 and 9. This irregular downward facing surface is the impetus for void creation.

To insure the best properties of a part created through the laser sintering process, layers must be processed in such a way as to minimize or eliminate voids between layers. Voided regions between layers define the fracture mode.

Effect of Reused Powder on Particle Melt

Based on the tensile data acquired, it was apparent that degraded powder did not yield poor mechanical properties when injection molded. This test gives us a good degree of confidence that the degradation of mechanical properties in the laser sintering process is not an intrinsic property defect but a property that affects the processing of the polyamide material in laser sintering.

Coplanar Void (h/r Ratio) Behavior

The existence of an interface boundary layer can be illustrated in Figures 6 and 7 from the SEM images. In addition, work done at the University of Louisvilleⁱ with microtoming and optical microscopy of samples shows evidence of a boundary region between layers. The work cited here and in Figures 20 and 21 have yet to be officially published at the time of this writing.

The images obtained from the University of Louisville show a cross section in a sample that is oriented the same as the fractures shown in Figure 6. The samples were created by using a microtoming technique common in medical pathology. The samples were sliced in layers roughly 5 microns thick to evaluate individual layers. It can be seen in Figures 20 and 21 that the fused layers (lighter color) are fully dense and the particles at the bottom of the layer (darker) are nylon particles that were not sintered. It can also be observed that there are



Figure 20: Optical Microscopy in a Bright Field (5X)

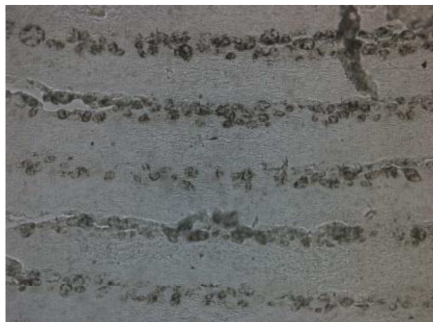


Figure 21: Optical Microscopy in a Bright Field (10X)

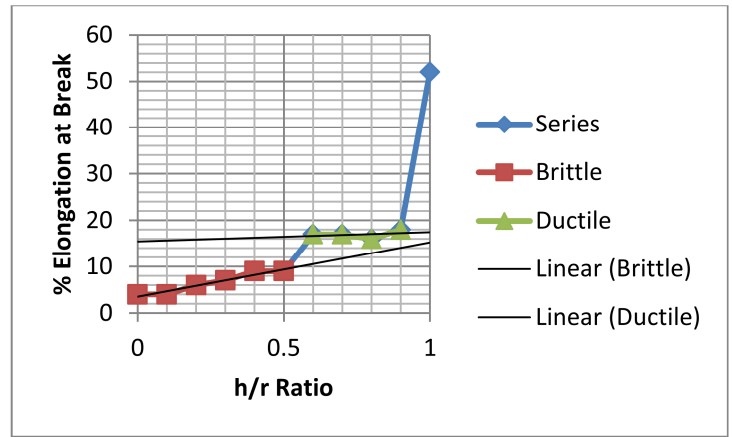


Figure 19: Trends in h/r Tensile Properties

several tears in the sample shown in Figure 20 that correspond with these darker (unmelted) regions.

When analyzing the graph in Figure 19, there are two distinct regions present (ductile and brittle). An h/r Ratio of 0 to 0.2 represent fracture before strain hardening which is seen in laser sintering as delamination. In addition, There is a grouping of these regions as illustrated in the stress-strain curve in Figure 16.

The use of an h/r Ratio helps quantify the failure modes in a macro scale and can help in identifying material process improvements that may help on a micro scale. This correlation is significant.

CONCLUSIONS

Thermally degraded powder does not affect the tensile properties when used in the injection molding process. Therefore, poor viscosity powders affect the laser sintering process negatively.

Poor layer-to-layer adhesion contributes to the formation of an interface boundary layer. This is evident in both SEM and optical microscopy.

The primary cause of the lower mechanical properties in the Z-axis can be attributed to layer-to-layer adhesion.

There are three distinct modes of failure in laser sintered specimens: delamination, brittle fracture, and ductile fracture.

It is apparent from the analysis of these samples that the cracks propagate through voids created by a lack of full melt between layers.

The use of an h/r Ratio helps qualify the regions of fracture.

An h/r Ratio of 0.6 demonstrates a shift between brittle and ductile fracture modes.

There is a major jump in mechanical properties when the interface boundary layer is significantly minimized between the 0.9 and 1.0 h/r Ratio region.

ⁱ Timothy J. Gornet, *pri.conv.*, University of Louisville